# Light Propelled Nanovehicles for Drug Delivery

Ana Marta Cabral, Prof. Dr. José Paulo Sequeira Farinha[1]

[1] Supervisor, Instituto Superior Técnico, Universidade de Lisboa, Portugal

November 2022

**Abstract:** The interest in nanocarriers for controlled and intelligent cargo delivery systems has increased due to the in versatility and tunability, offering extremely promising opportunities within this field. These can already address very well-defined morphology, large cargo capacities, targeting of the destination, and on-demand controlled delivery. The goal of this project was to add self-propulsion capabilities to these nanovehicles, transforming them in versatile nanorobotic tools. Our proof-of-concept nanovehicles are Janus nanoparticles (JNPs) composed by a silica nanoparticle core and a gold nanostructure in half of their surface. Upon irradiation, the vehicle is propelled in the opposite direction of the gold nanoshell by a photothermal effect. Our proof-of-concept system exhibited a strong plasmon optical resonance. Upon irradiation with a 632.8 nm laser, it showed the occurrence of two diffusion regimes: translational and rotational. The average directional velocity reached by this system was 3.95 μm/s.

**Keywords:** Janus nanoparticles, gold nanoparticles, silica nanoparticles, Pickering emulsion, plasmon resonance, self-propulsion.

## 1 Introduction

Janus particles are anisotropic materials that allow the emergence of properties inconceivable for symmetric or homogeneous particles. Their morphologies range from spherical particles to different shapes such as dumbbell-shape, disk-shape and rod-shape.[1,2] They can be classified into three categories: polymeric, inorganic and hybrid polymeric-inorganic Janus particles.[3] Due to the in anisotropic structure, distinct morphologies and compositions, Janus particles can be used in diverse applications, including solid surfactant agents, micro/nanomotors with controlled movement and biomedical applications.[3]

Inorganic Janus particles can be prepared by masking, which is accomplished by either trapping the particles at the interface between two phases or by depositing or adsorbing them on a solid substrate. The entrapment between different phases can be done in emulsions. Pickering emulsions are emulsions stabilized by solid particles, and have been widely used in the preparation of Janus particles.[4,5] The effectiveness of Pickering emulsions is determined by the degree of wettability of the solid particles, since their adsorption at the oil-water interface is influenced by its hydrophobicity. The wettability of the solid particles can be tailored by surface functionalization.[6]

Self-propulsion is achieved when micro/nanomotors are capable of converting different sources of energy, such as electromagnetic radiation, into kinetic energy. Most present an asymmetric structure, which allows them to achieve spontaneous directional motion. Light-driven motors are easily controlled by light intensity, present a fast response to light irradiation as well as long-term motion, and can be classified according to the type of mechanism responsible for propulsion: self-electrophoretic, self-diffusiophoretic, thermophoretic or bubble-induced propulsion.[7,8] In the case of metallic nanomaterials, the electromagnetic energy is converted into heat through the surface plasmon resonance process, i.e., the heat is produced by a joule dissipation of oscillating electrons.[9]

The particular case of silica-gold Janus nanoparticles is very promising due to their properties and versatility for changing the geometry and shell morphology. Silica nanoparticles (SNPs) can be prepared by sol-gel methods and can posteriorly have their surface easily modified with functional groups to strongly increase their interaction with gold nanoparticles (AuNPs). The growth of a gold nanoshell on a silica core can be achieved by a seeding method, where the shell is grown on a modified silica core with deposited AuNPs. The plasmon resonance of the gold nanoshell can be easily tuned from visible to NIR range of the electromagnetic spectrum, by varying the aspect ratio of the shell thickness to the core diameter.[10]

In a typical approach, SNPs are surface modified with 3-aminopropyl triethoxysilane (APTES), ensuring the saturation of the surface of the SNPs with APTES, in order to provide enough $NH_2$ groups that could link to gold nanoparticle seeds. Figure 1 shows the synthetic procedure of core-shell silica-gold nanoparticles. The growth of the gold shell on the seeded surface can be done using different reducing agents: formaldehyde, ascorbic acid, or sodium borohydride.

The growth of a half gold nanoshell on SNPs originates a Janus nanoparticle, that undergoes translational diffusion and rotational (Brownian) diffusion.[11]

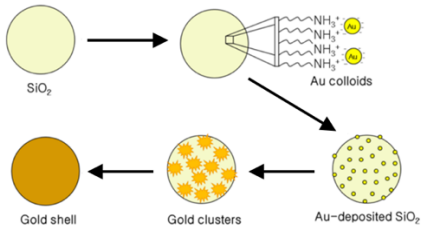

Figure 1: Schematic representation of the synthesis of core-shell silica-gold nanoparticles. Adapted from [12]

The motion can be investigated by dynamic light scattering (DLS). Scattering of coherent monochromatic radiation by a group of particles originates interference of scattered light which leads to intensity fluctuations in time. The particle mobility can be determined by correlating the intensity fluctuations of the scattered radiation at a constant angle.
Anisotropic particles exhibit, at long decay times, a step in the autocorrelation curve and a constant $\Delta L^2$, indicating rotational diffusion. While at short decay times, $\Delta L^2$ exhibits a power-law slope, which is characteristic of translational diffusion.[13]

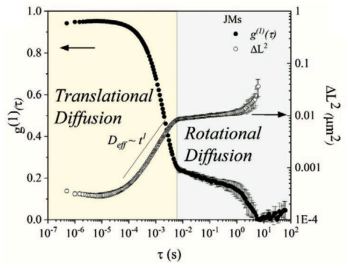

Figure 2: Autocorrelation and $\Delta L^2$ of anisotropic particles versus decay times.[13]

The average directional speed of anisotropic particles is is the apparent translation diffusion coefficient under irradiation ($D_{eff}$), the translation diffusion coefficient without irradiation (corresponding to Brownian motion, $D_0$), and the rotation relaxation time ($\tau_R$).
Herein, we present Janus nanoparticles, composed by a silica core and a gold halfshell, prepared via a Pickering emulsion route. The aim is to add self-propulsion capabilities to nanovehicles, transforming them in versatile nanorobotic tools for drug delivery applications. The optical properties and movement under irradiation of the Janus nanoparticles were studied by UV/Vis spectroscopy and Dynamic Light Scattering.
SNPs were used to stabilize Pickering emulsions and their exposed surface was functionalized with APTES, saturating the surface and providing enough $NH_2$ groups to link gold nanoparticle seeds into a halfshell. Due to the presence of the gold halfshell, the absorption spectrum of the Janus nanoparticles exhibits a plasmon resonance wavelength, which can be tuned by varying the thickness of the shell.
Under irradiation, the system is expected to produce a temperature gradient on the gold halfshell side due to the photothermal effect, acquiring self-propulsion.

# 2 Experimental Part

## 2.1 Materials

For the synthesis of Stöber SNPs were used absolute ethanol (Honeywell), ammonium hydroxide solution ($NH_4OH$ basis, 28.0-30.0%, Aldrich) and tetraethyl orthosilicate (TEOS, ≥ 99.0%, Aldrich). The deionized (DI) water used was generated by a Millipore Milli-Q system ≥ 18 MΩcm (with a Millipak membrane filter 0.22 µm). Pickering emulsions were produced with SNPs, distilled water, hexadecetyltrimethylammonium bromide (CTAB, ≥99%, Sigma) and paraffin wax (melting point 53-58 °C, Sigma-Aldrich). To dissolve paraffin wax, chloroform (> 99.8%, Sigma-Aldrich) was used. SNPs were surface modified with 3-aminopropyl triethoxysilane (APTES, 99%, Aldrich) in methanol (CIL) and in a mixture of absolute ethanol (Honeywell) and ammonium hydroxide solution ($NH_4OH$ basis, 28.0-30.0%, Aldrich). Argon (Ar) (≥ 99.9999%) used was from Alphagaz Air Liquide. To prepare the NMR analysis samples, 1,3,5-trioxane (≥ 99%, Fluka), deuterium oxide (D2O, 99.9% atom, CIL) and sodium hydroxide (pure NaOH, EKA pellet) were used. AuNPs were synthesized with deionized (DI) water, gold (III) chloride trihydrate (≥ 99%, Aldrich), sodium citrate dihydrate (≥ 99%, Aldrich) and sodium borohydride (> 98.5%, Aldrich). The deposition of AuNPs was done using absolute ethanol (Honeywell) and sodium chloride (Merck). The growth of the gold nanoshell was promoted using potassium carbonate (> 99%, Aldrich), deionized (DI) water, gold (III) chloride trihydrate (≥ 99%, Aldrich), formaldehyde solution (36.5-38% in H2O, Sigma-Aldrich), sodium citrate dihydrate, ascorbic acid (99%, Sigma-Aldrich) and sodium borohydride (> 98.5%, Aldrich).

## 2.2 Synthesis of Stöber Silica Nanoparticles

In a polypropylene flask, absolute ethanol (866.56 g), Milli-Q water (90.21 g) and $NH_4OH$ (15.1 mL) were added and stirred at 40°C. After, TEOS (44.6 mL) was added to the mixture, and left overnight. After cooling, the dispersion was centrifuged (90 000G, 20 minutes) and washed three times with absolute ethanol. The nanoparticles were dried at 60°C in a ventilated oven overnight.

## 2.3 Production of Pickering Emulsions

200 mg of SNPs were dispersed in 15 mL of distilled water. Then, CTAB was introduced at a concentration below the critical micellar concentration (~CMC/5, the

critical micellar concentration of CTAB in water at room temperature is 0.92 mM).
The mixture is heated at 75°C, and 400 mg of molten paraffin are added drop by drop while maintaining vigorous stirring by means of an Ultra-Turrax homogenizer. A final stirring is accomplished by applying strong shear induced with an Ultra-Turrax.
The emulsions are cooled down to a temperature below the melting point of paraffin, CTAB is added to reach its critical micellar concentration, further stabilizing the paraffin dispersion.
The final dispersion was let to settle, and the supernatant was removed. After, the paraffin droplets stabilized by SNPs were recovered by centrifugation (80 000G, 15 minutes) and washed two times with water, they were dried at room temperature.

## 2.4 Surface Functionalization of Silica Nanoparticles

For the surface functionalization of SNPs, 3-aminopropyl triethoxysilane (APTES) was used. Initially, the quantity of APTES was tailored to obtain 2 molecules per $nm^2$ on the surface of the SNPs. Later, it was tailored to obtain 15 molecules per $nm^2$.
*Homogeneous surface modification:* 250 mg of SNPs were dispersed in methanol (7 g) at room temperature. In another experiment, the same quantity of SNPs was dispersed in 15 mL of ethanol/aqueous ammonia mixture (7%, v/v) at room temperature. Then, APTES was added to the mixture and it was maintained at room temperature and under argon atmosphere during 48 hours. The nanoparticles were recovered by centrifugation and washed four times with absolute ethanol (70 000G, 10 minutes). They were dried at 60°C in a ventilated oven overnight.
The quantity of APTES to reach 2 and 15 molecules of APTES per $nm^2$ is 10.6 and 79.53 mg of APTES, respectively.
*Half surface modification:* To accomplish a half surface modification of SNPs with APTES, the total amount of paraffin droplets stabilized by SNPs were dispersed in methanol (7 g) at room temperature. Then, APTES was added and the mixture was maintained at room temperature and under argon atmosphere during 48 hours. Assuming that SNPs are immersed in paraffin droplets and only half of their surface is exposed, the quantity of APTES required in the functionalization, in order to obtain 2 molecules of APTES per nm2, was 4.24 mg.
In another experiment, the total amount of paraffin droplets stabilized by SNPs were dispersed in 15 mL of ethanol/aqueous ammonia mixture (7%, v/v) at room temperature. Then, excess APTES (79.53 mg) was added, the mixture was maintained at room temperature and under argon atmosphere during 48 hours. In this case, the quantity of APTES was not determined based on the previous assumptions.
The resultant particles were washed three times with absolute ethanol (70 000G, 10 minutes). The paraffin was then dissolved with chloroform, the mixture was centrifuged (5 000 rpm, 20 minutes) and the SNPs were recovered by centrifugation and submitted to a final washing with absolute ethanol (70 000G, 10 minutes). The particles were dried at 60°C in a ventilated oven overnight.

## 2.5 Synthesis of Gold Nanoparticles

645 µl of 1% (w/v) sodium citrate were added to 100 mL of 0.01% (w/v) $HAuCl_4$ under vigorous stirring at room temperature. After 3 minutes, 3 mL of 0.1 M NaBH4, prepared in ice-cold water, was added to the mixture. The color of the solution changes immediately from colorless to red (figure 19). After 30 minutes of stirring, the colloidal solution was left for 2 hours without stirring at room temperature. The AuNPs were stored in a polypropylene flask at 4°C for further use.

## 2.6 Deposition of Gold Nanoparticles onto Silica Nanoparticles

AuNPs were deposited onto the SNPs in the absence and presence of NaCl.
For the deposition without NaCl, 43 mg of surface modified SNPs were dispersed in 0.5 mL of absolute ethanol with sonication and introduced in a centrifuge tube with 16 mL of the AuNPs solution. The dispersion was gently stirred overnight, centrifuged (15 300 rpm, 5 minutes), and washed four times with water. The resultant nanoparticles were dried at 60°C in a ventilated oven overnight.
For the deposition in the presence of NaCl, 29.25 mg of surface modified SNPs were dispersed in 1.5 mL of ethanol with sonication and introduced in a flask with the AuNPs solution and a 1 M NaCl solution. The dispersion was gently stirred overnight, centrifuged (15 300 rpm, 5 minutes), and washed four times with water. The particles were redispersed in 3 mL of water.

## 2.7 Growth of Gold Nanoshell

The growth of the gold nanoshell was attempted by three different approaches.
*Reduction with formaldehyde:* Initially, two solutions containing potassium carbonate ($K_2CO_3$) and chloroauric acid were prepared. The preparation of the first solution, called as K-gold1, involved the dissolution of 25 mg of potassium carbonate in 100 mL of deionized water by stirring during 10 minutes. Then, 1.5 mL of a solution of 1% $HAuCl_4$ in water was added and it was left to stir overnight. While for the second solution, called as K-gold2, 60 mg of potassium

carbonate and 1.5 mL of 25 mM of $HAuCl_4$ were dissolved in 100 mL of deionized water. This solution was left to stir during 1 day. During both aging periods, the color of the solutions changed from yellow to transparent.

The gold nanoshell was first grown by dispersing 18 mg of gold nanoparticle seeded SNPs in 0.5 mL of milli-Q water, and adding it to 20 mL of K-gold1 solution while stirring. Then, 10 µL of a formaldehyde solution was added, and the solution become purple in less than 2 minutes. It was left stirring for 30 minutes. The solution was centrifuged (15 300 rpm, 5 minutes) and washed three times with water. The resultant nanoparticles were dried at 60°C in a ventilated oven overnight.

The growth of a gold nanoshell was also attempted at 55°C and room temperature. In the first method, 10 mL of K-gold2 solution and 200 µL of jSNP5_Au1 dispersion were mixed at 55°C during 10 minutes. Then, 25 µL of a formaldehyde solution was added and the solution was mixed for 15 minutes. The second method was performed at room temperature, in which 800 µL of K-gold2 solution and 9.2 mL of milli-Q water were mixed. Then, 250 µL of half gold seeded silica nanoparticles dispersion were added, and the solution was mixed for 10 minutes. 40 µL of formaldehyde solution was added at the end and the solution was mixed for 15 minutes. Both final solutions were centrifuged (15 300 rpm, 5 minutes) and washed three times with water, and redispersed in 10 mL of milli-Q water.

*Reduction with sodium borohydride:* Briefly, 50 mL of K-gold2 solution was heated to 50°C, and left to stir during 5 minutes. 100 µL of half gold seeded silica nanoparticles dispersion were added and the solution was mixed vigorously during 10 minutes. Then, 2.5 mL of 10 mM sodium citrate solution was added. And after 1 minute, 5 mL of 6.6 mM sodium borohydride solution (250 µL in 1-minute intervals) was added. Upon each addition of the sodium borohydride solution, the solution changed to a more pronounced purple color. The solution was mixed during 15 minutes, centrifuged (15 300 rpm, 5 minutes) and washed three times with water, and redispersed in 10 mL of milli-Q water.

*Reduction with ascorbic acid:* A 0.75 wt% sodium citrate solution was added to a 1.92 mM $HAuCl_4$ aqueous solution. Then, a dispersion of gold seeded SNPs was added. And finally, a 4 mM ascorbic acid aqueous solution was added.

### 2.8 Characterization

$^1H$ NMR spectra was obtained by a Bruker Avance III 400 spectrometer (Bruker BioSpin GmbH, Rheinstetten, Germany) operating at 400 MHz. Zetasizer Nano ZS (Malvern, model ZEN3600), with a 632.8 nm laser, was used to determine the hydrodynamic diameter and to perform the propulsion studies. For the propulsion studies, each sample was agitated during 2 minutes before executing the measurement. T18 digital Ultra-Turrax (IKA) and T25 easy clean digital Ultra-Turrax (IKA) were used to produce Pickering emulsions. Absorption spectra were obtained by Jasco V-660 UV-VIS Spectrophotometer (Oklahoma City, OK, USA) with a double monochromator and photomultiplier tube detector for higher resolution was used to obtain the absorbance spectra. The measurements were carried out in disposable cells at room temperature. Transmission Electron Microscopy (TEM) images were captured with a Hitachi transmission electron microscope (Hitachi High Technologies, Tokyo, Japan), model H-8100, with a LaB6 filament (Hitachi) complemented with an accelerator voltage of 200kV. An incorporated camera KeenView (Soft Imaging System, Münster, Germany) was used to acquire TEM images.

## 3 Results and Discussion

### 3.1 Synthesis and Characterization of Silica Nanoparticles

SNPs were synthesized by the Stöber method and the particle size was evaluated by means of DLS and TEM. The average diameters obtained from DLS and TEM are (69 ± 19) nm and (66 ± 8) nm, respectively. Since DLS measures the hydrodynamic diameter, it accounts for the nanoparticle diffusion within a fluid; hence the hydrodynamic diameter is slightly higher than the diameter measured by TEM because of the particle solvation sphere. Figure 3 shows the spherical morphology and uniform size distribution of the SNPs synthesized.

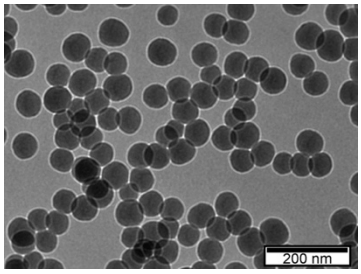


Figure 3: TEM image (scale bar: 200 nm) of SNPs. D = (66 ± 8) nm.

### 3.2 Production and Characterization of Pickering Emulsions

Emulsions consisting of water and paraffin wax were stabilized by SNPs which were made partially hydrophobic by adsorbing CTAB. Its adsorption allows tuning the penetration depth of the particles in the paraffin droplets. After the emulsification process, the emulsions undergo sedimentation, caused by density differences between water and paraffin droplets

stabilized by SNPs. The expected droplet diameter is calculated, assuming that half of each SNP penetrates the paraffin droplet, that all the SNPs are stabilizing the paraffin droplets and that all paraffin wax was emulsified. The expected and obtained droplet diameters are presented in table 1, as well as the conditions used.

Table 1: Conditions of the Pickering emulsions, and expected and obtained droplet diameter.

| Sample | SNPs (mg) | Paraffin Wax (mg) | Ultra-Turrax Speed (rpm) | Expected Droplet Diameter (µm) | Obtained Droplet Diameter (µm) |
|---|---|---|---|---|---|
| jSNP1 | 200 | 400 | 9 000 | 4.6 | 10 ± 3 |
| jSNP2 | 150 | 400 | 9 000 | 8.2 | * |
| jSNP3 | 100 | 400 | 9 000 | 18.5 | * |
| jSNP4 | 200 | 400 | 10 600 | 4.6 | 5 ± 1 |
| jSNP5 | 200 | 400 | 10 600 | 4.6 | 3.5 ± 0.7 |
| jSNP6 | 200 | 400 | 12 000 | 4.6 | 8 ± 4 |

* These values were not calculated because no droplets were formed.

For jSNP1, larger droplets were obtained, which can indicate that a lack of SNPs has been used or that the Ultra-Turrax speed was not enough to induce a strong shear in order to homogenize the emulsions.
As the mass of SNPs used decreases (jSNP2 and jSNP3), larger droplets are expected. However, when visualizing jSNP2 and jSNP3 by means of an optical microscopy, no larger droplets were formed. By maintaining the initial conditions of SNPs and paraffin wax, and increasing the speed of the Ultra-Turrax from 9 000 to 10 600 rpm, in order to induce a stronger shear that is expected to create smaller droplets, droplets with a diameter of (5 ± 1) µm were obtained (figure 4).

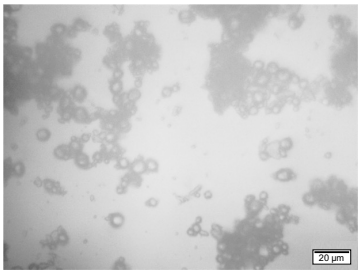


Figure 4: Optical microscopy image (scale bar: 20 µm) of jSNP4. Obtained droplet diameter is (5 ± 1) µm.

For jSNP5, smaller droplets were obtained (figure 5A), suggesting that not all the paraffin wax was involved in the emulsification process, which is confirmed in figure 5B where paraffin wax is visible in the upper walls of the flask. Increasing the speed of the equipment from 10 600 to 12 000 rpm induced more shear and allowed to obtain a more uniform distribution of droplets with larger sizes (jSNP6).

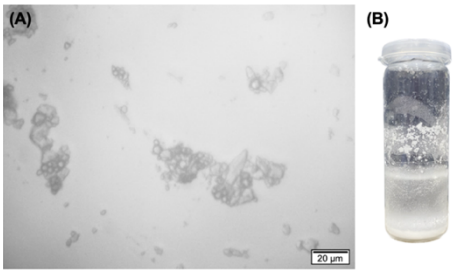


Figure 5: (A) Optical microscopy image (scale bar: 20 µm) of jSNP5. Obtained droplet diameter is (3.5 ± 0.7) µm. (B) Flask in which jSNP5 was produced.

## 3.3 Surface Functionalization of Silica Nanoparticles

SNPs were surface modified with 3-aminopropyl triethoxysilane (APTES) to promote the deposition of gold nanoparticle seeds. The functionalization quantification was carried out via $^1$H NMR as described by our group.[14] An internal standard (trioxane) is used in the quantification. Through comparison of the integrated intensity of the trioxane peak and the peaks corresponding to the $CH_3$ and $CH_2$ protons of APTES, the number of APTES molecules grafted per nm$^2$ in the SNPs was estimated (table 2).

Table 2: Functional group quantification by NMR.

| Sample | [APTES] mmol/$g_{SNP}$ | Target Surface Coverage (molecules/nm$^2$) | Experimental Surface Coverage (molecules/nm$^2$) |
|---|---|---|---|
| SNP1_f | 0.49 | 2 | 5.1 |
| SNP2_f | 0.25 | 15 | 2.6 |
| SNP3_f | 0.54 | 15 | 5.6 |
| jSNP1_f | 0.050 | 2 | 1.1 |
| jSNP4_f | 0.073 | 2 | 1.5 |
| jSNP5_f | 0.76 | 15 | 16 |
| jSNP6_f | 0.50 | 15 | 10 |

The target surface coverage was only reached for jSNP5_f. When functionalizing the total surface of SNPs, the quantity of APTES was tailored to have a surface coverage of 2 molecules per nm$^2$, to ensure a good functionalization without overlapping of APTES. However, that was not enough to guarantee a high AuNP seed deposition density. Hence, the surface coverage was tailored to 15 molecules per nm$^2$. The functionalization in an ethanol/aqueous ammonia mixture (SNP1_f and SNP2_f) resulted in a higher surface coverage of APTES than in methanol (SNP3_f), because ammonia leads to the hydrolysis of APTES and to its efficient condensation on the SNPs surface. In the case of half surface modification (jSNP1_f, jSNP2_f, jSNP3_f and jSNP4_f), the quantity of APTES was tailored to deliver 2 molecules per nm$^2$. Lower surface coverages were obtained, which can be justified by a low penetration depth of the

SNPs in the paraffin droplets. If more than half of the SNP surface is exposed and the quantity of APTES is tailored for 2 molecules per $nm^2$, then it is expected to have less than that value of surface coverage. As mentioned before, the surface coverage was tailored to 15 molecules per $nm^2$ for the half surface modification, and higher surface coverages (jSNP5_f and jSNP6_f) were obtained because excess of APTES was used.

### 3.4 Synthesis and Characterization of Gold Nanoparticles

AuNPs were synthesized by reduction of $HAuCl_4$ with sodium borohydride ($NaBH_4$) in the presence of sodium citrate. $NaBH_4$ acts as the reductor agent and sodium citrate as a stabilizing agent. The particle size was evaluated by TEM, and the absorption spectrum was acquired by UV/Vis Spectroscopy. The absorption spectrum (figure 6A) was obtained, and the SPR wavelength of the AuNPs is at 507 nm. Figure 6B shows the spherical morphology and uniform size distribution of the AuNPs synthesized. The average diameter of the AuNPs is (4.9 ± 0.6) nm.

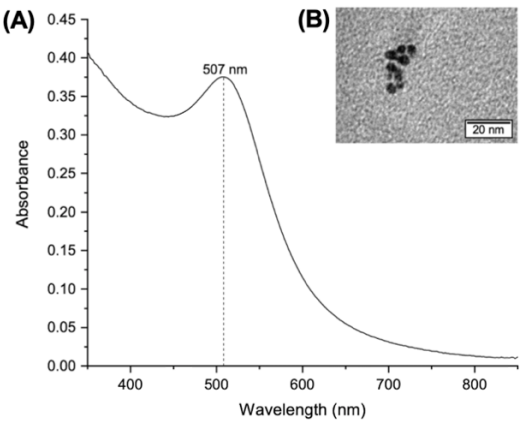


Figure 6: (A) Absorption spectra of AuNPs. (B) TEM image (scale bar: 20 nm) of AuNPs. D = (4.9 ± 0.6) nm.

### 3.5 Deposition of Gold Nanoparticles on Silica

After the functionalization step, AuNPs were deposited onto the surface of the SNPs in the presence and absence of NaCl. The gold seeded SNPs were then analyzed by UV/Vis Spectroscopy and TEM. The AuNP seed deposition density is influenced by the surface coverage (APTES molecules/$nm^2$), volume of AuNPs solution used and presence of NaCl during deposition. Higher surface coverage translates into more $NH_2$ groups available to link to AuNPs. Also, an excess of AuNPs solution must be used, in order to ensure that all $NH_2$ groups are linked to AuNPs. With respect to NaCl, it reduces the electrostatic repulsion of the particles, allowing a higher AuNP seed deposition density. The presence of NaCl is responsible for an increased ionic strength; therefore, SNPs covered with amine groups will protonate more, allowing the adsorption of negatively charged AuNPs onto the positively charged surface of SNPs.

SNPs that exhibit high AuNP seed deposition density are expected to exhibit a more pronounced red shift of the absorbance peak. The wavelengths of maximum absorbance are presented in table 3, along with the parameters influencing the deposition.

Table 3: Conditions of the AuNPs deposition and absorbance peaks (nm) obtained.

| Sample | Experimental Surface Coverage | AuNPs (mL) | NaCl | Absorbance Peak (nm) |
|---|---|---|---|---|
| SNP3_Au1 | 5.61 | 38.5 | ✓ | 534 |
| SNP3_Au2 | 5.61 | 68.5 | ✓ | 556 |
| jSNP1_Au1 | 1.05 | 16 | — | 523 |
| jSNP4_Au1 | 1.52 | 16 | — | 524 |
| jSNP5_Au1 | 15.81 | 80 | ✓ | 534 |
| jSNP6_Au1 | 10.36 | 80 | ✓ | 542 |

The half gold seeded SNPs obtained by Pickering emulsification, jSNP1_Au1 and jSNP4_Au1 resulted from the deposition of AuNPs without NaCl onto SNPs with similar and low surface coverage of APTES per $nm^2$, and exhibited absorbance peaks at around the same wavelength. While jSNP5_Au1 and jSNP6_Au1 were synthesized from SNPs with high surface coverage of APTES per $nm^2$, and more AuNPs were deposited in the presence of NaCl. Therefore, the combination of higher surface coverages and deposition with NaCl to reduce the repulsions of the particles allowed a more efficient adsorption of AuNPs to the SNPs surface. And their absorbance peaks red shifted in comparison to jSNP1_Au1 and jSNP4_Au1. However, the shift was not as pronounced as it was for SNP3_Au2 (table 3), because, for jSNP1_Au1 and jSNP4_Au1, only half of the SNPs surface had AuNPs adsorbed. The optical properties of the gold nanoshells vary with the shape factor. As it increases, the plasmon resonance is red-shifted.[15,16] The absorbance peak of jSNP6_Au1 is more red shifted than that of jSNP5_Au1, even though jSNP6_Au1 exhibited lower surface coverage of APTES. However, the obtained surface coverage is only an estimative because an assumption that all the SNPs were half penetrated in the paraffin droplets was made. In addition, the number of SNPs that were stabilizing the paraffin droplets is uncertain.

TEM images of jSNP5_Au1 and jSNP6_Au1 (figures 7 and 8) show evidence of areas of the SNPs surface not covered by AuNPs. However, some particles appear to be fully covered with AuNPs, which can be explained by how the particle is positioned on the grid relative to

the electron beam. Other possibility to the appearance of those can be that, during the Pickering emulsification, SNPs were not stabilizing paraffin droplets and therefore were completely surface modified with APTES, enabling the deposition of AuNPs onto the total surface of SNPs. On the other hand, in figure 7, SNPs without AuNPs are also visible, which can be justified by a total penetration of some SNPs into the paraffin droplets, impeding the half surface modification of the SNPs. From figures 7 and 8, less than half of the SNPs surface is not covered with AuNPs, which is justified by the production of Pickering emulsions, indicating that SNPs were only partially penetrated in the paraffin droplets.

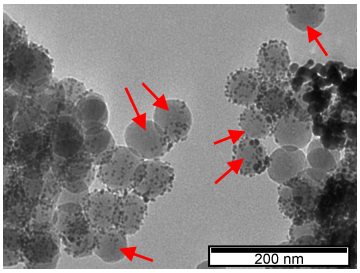


Figure 7: TEM image (scale bar: 200 nm) of jSNP5_Au1. Red arrows indicate areas not covered by AuNPs.

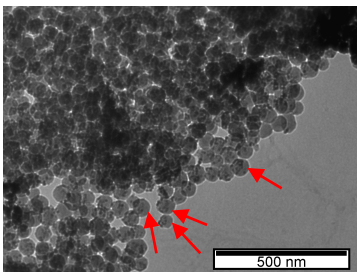


Figure 8: TEM image (scale bar: 500 nm) of jSNP6_Au1. Red arrows indicate areas not covered by AuNPs.

### 3.6 Growth of Gold Nanoshell

The growth of the gold nanoshell was performed by using different concentrations of a reducible gold salt ($HAuCl_4$) with different reducing agents (ascorbic acid, $NaBH_4$ and formaldehyde).

The gold nanoshell was grown in SNP3_Au1 and SNP3_Au2, originating SNP3_Au3 and SNP3_Au4, respectively. It resulted in an 8 nm and 7 nm shift of the absorbance peaks for SNP3_Au3 and SNP3_Au4, respectively, in comparison to the absorbance peaks of the gold seeded SNPs. The growth did not create a uniform nanoshell, which can be justified by a low concentration of $HAuCl_4$ in solution during growth. To achieve a more complete and uniform gold nanoshell, it would have been necessary to increase the surface coverage of APTES per $nm^2$ of SNPs. The reducing agents used to grow an isotropic gold nanoshell and the absorbance peaks obtained by UV/Vis Spectroscopy are presented in table 4.

Table 4: Reducing agents used to grow the gold nanoshell and absorbance peaks (nm) obtained.

| Sample | Reducing Agent | Absorbance Peak (nm) |
|---|---|---|
| SNP3_Au3 | Ascorbic acid | 542 |
| SNP3_Au4 | Ascorbic acid | 563 |

Half gold seeded SNPs with low surface coverage of APTES (jSNP1_Au2, jSNP1_Au3 and jSNP4_Au2) exhibited a poor growth of the nanoshell via reduction with formaldehyde. The low surface coverage resulted in a reduced number of AuNPs adsorbed at the surface, which were not sufficient to act as nucleation sites for reduction of gold and creation of a half nanoshell. After a first growth on jSNP1_Au2 and jSNP4_Au2, the absorbance peaks (figure 9) were at around the same wavelength despite the fact that jSNP4_Au2 presented large APTES surface coverage (1.52 molecules/$nm^2$), which was expected to increase the AuNP seed deposition density in comparison to jSNP1_Au2. A second growth of jSNP1_Au3 was performed and resulted in a red shift of 10 nm in comparison to the first growth, indicating that there was reduction of gold on the AuNPs seeded in the SNPs.

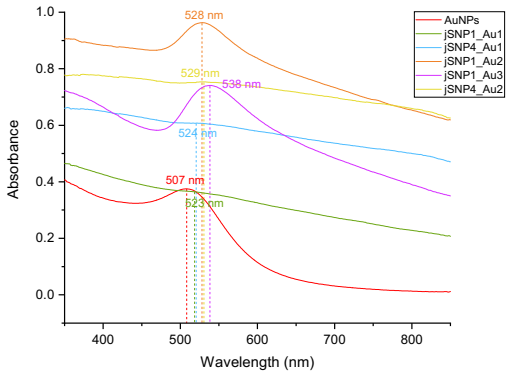


Figure 9: Absorption spectra of core-shell silica-gold NPs.

Half gold seeded SNPs with the highest surface coverage of APTES (15.81 molecules/$nm^2$) exhibited different behaviors upon the growth of the nanoshell by reduction with different reducing agents, which can be verified by the position of the absorption peaks (figure 10).

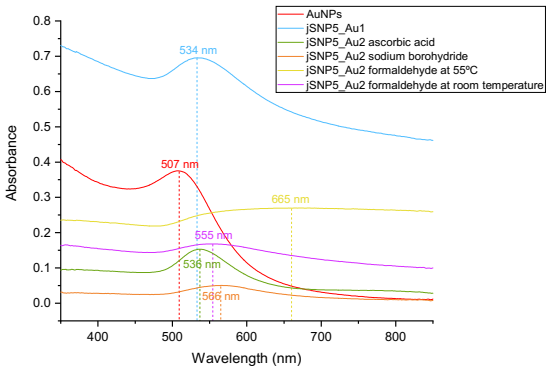


Figure 10: Absorption spectra of half gold nanoshell SNPs, in which the nanoshell was grown using different reduction mechanisms.

The reduction of $HAuCl_4$ with ascorbic acid caused a 2 nm red-shift of the absorbance peak. However, from figure 11, it is visible that larger AuNPs were formed during this process. And it is safe to assume that those are not SNPs with a gold nanoshell, because of the reduced red-shift, confirming that no gold nanoshell was formed.

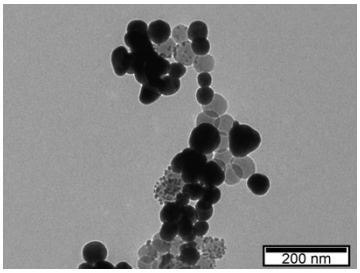


Figure 11: TEM image (scale bar: 200 nm) of jSNP5_Au2 grown by reduction of chloroauric acid with ascorbic acid.

Regarding the formation of a half gold nanoshell by reduction with $NaBH_4$, it is clear that the previously AuNPs seeded to the SNPs surface did act as nucleation sites for reduction of gold (figure 12).

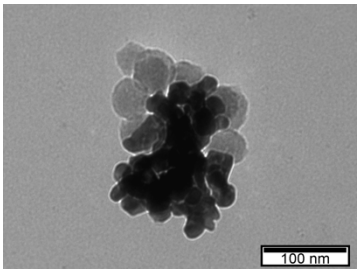


Figure 12: TEM image (scale bar: 100 nm) of jSNP5_Au2 grown by reduction with $NaBH_4$.

However, a non-uniform nanoshell was created, which can be justified by the addition of excess of $NaBH_4$ solution. Perhaps, a more uniform half gold nanoshell could have been obtained by adding less $NaBH_4$ solution, and its growth could have been controlled upon each addition of the reducing solution. This growth resulted in a 32 nm red shift with respect to the half gold seeded SNPs, indicating that the seeded AuNPs have grown into larger particles and coalesced. The growth of a half gold nanoshell was also accomplished by reduction with formaldehyde at 55°C and at room temperature. At 55°C, the growth of the half gold nanoshell was successfully accomplished (jSNP5_Au2). Figure 13 shows that an almost uniform nanoshell has grown and that the nanoshell was not created in some areas of the SNP surface. AuNPs seeded to the SNPs surface acted as nucleation sites for reduction of gold, and AuNPs have grown into larger particles, which has decreased the distance between them, leading to the plasmon coupling between neighboring AuNPs. This has a result in a 131 nm red-shift of the absorbance peak, indicating the formation of a nanoshell. At room temperature, the previously AuNPs seeded to the SNPs surface appear to have grown non-uniformly (figure 14). The seeded AuNPs acted as nucleation sites, but it appears that nucleation only occurred in specific areas, and not in every AuNP seeded to the SNPs surface. Nevertheless, a 21 nm red-shift was verified, indicating that, for jSNP5_Au2, AuNPs have grown but a half gold nanoshell was not created.

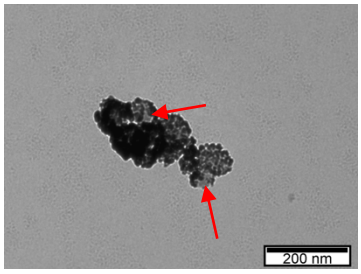


Figure 13: TEM image (scale bar: 200 nm) of jSNP5_Au2 grown by reduction with formaldehyde at 55°C.

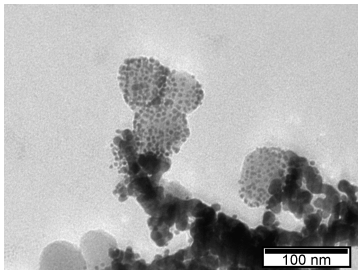


Figure 14: TEM image (scale bar: 100 nm) of jSNP5_Au2 grown by reduction with formaldehyde at room temperature.

From all the approaches, using formaldehyde as a reducing agent at 55°C resulted in the growth of the more uniform nanoshell. The control over the shell thickness can be made by varying the amount of reducing agent used and the temperature during growth. The addition of 25 µl of a formaldehyde solution at 55°C allowed the formation of a nanoshell, while the addition of 40 µl of a formaldehyde solution at room temperature contributed to growth of AuNPs into larger particles. Therefore, temperature affects the growth of the nanoshell, more than increasing the amount of reducing agent used (formaldehyde). The preferrable approaches would be either using ascorbic acid or $NaBH_4$ as reducing agents, because of the toxicity issues associated with formaldehyde.

### 3.7 Motion Studies

The motion of the system was studied by means of DLS. The measurements were performed at 25°C, using the backscatter mode ($\theta = 173°$), because high angle measurements are more sensitive to the motion of moving colloids and any changes in their diffusive behavior.[13]

DLS measurements of SNPs, jSNP5_Au1 and jSNP5_Au2 (gold nanoshell grown with formaldehyde at 55°C) were executed, and the autocorrelation curves of jSNP5_Au1 and jSNP5_Au2 are represented in figure 15. Isotropic particles are known for presenting a single decay event in the autocorrelation function while anisotropic particles exhibit two distinct decay events. jSNP5_Au2 behave as isotropic particles, which is justified by an excessive growth of the nanoshell, that resulted in a decrease of the SNPs surface area not covered with AuNPs. While jSNP5_Au1 behave as anisotropic particles.

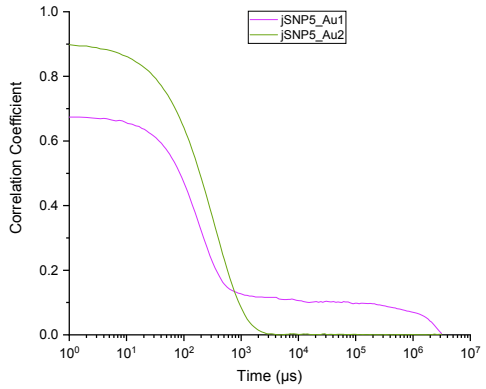


Figure 15: Autocorrelation function of jSNP5_Au1 and jSNP5_Au2.

For jSNP5_Au1, the rotational and translational diffusion is decoupled as two distinct decay events in the autocorrelation function. A fitting of that function using the difference of squares method and the Solver feature of Excel was done. The autocorrelation function that describes the behavior of jSNP5_Au1 was determined as:

$$g^{(1)}(\tau) = 0.59e^{-(5.65\times10^{-3})\tau} + 0.11e^{-(4.20\times10^{-7})\tau}$$

The values for $D_{eff}$ and $\tau_R$ are 8.13 µm²/s and 0.40 s, respectively. At short decay times, the first decay in the autocorrelation function of jSNP5_Au1 corresponds to the translational diffusion of the particles (figure 16). While the long decay times are limited to rotational diffusion. To confirm that these decays correspond to the translational and rotational regimes, the mean-squared displacement of the particles was determined. The autocorrelation function is related to the mean-squared displacement by equation 3, which can be rearranged to obtain a plot of $\Delta L^2$ versus decay time (figure 16).

At short decay times, $\Delta L^2$ is characterized by a power-law slope, which is characteristic for translational diffusion, while at long decay times, $\Delta L^2$ is constant, which describes the rotational diffusion regime.

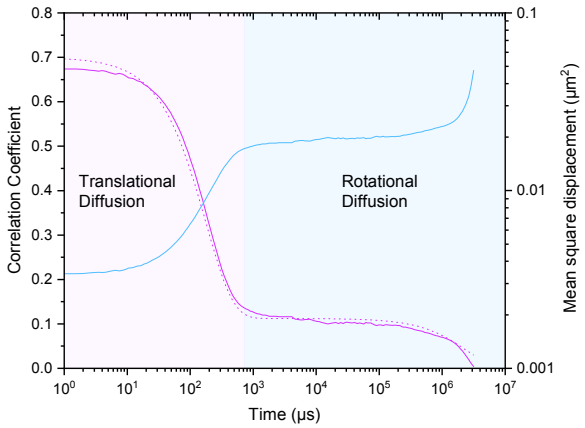


Figure 16: Autocorrelation function (purple line) and mean square displacement (blue line) versus decay time of jSNP5_Au1. Purple dots represent the fitting done for the autocorrelation function. Purple area of the plot corresponds to the translational diffusion regime that occurs at short decay times. Blue area of the plot corresponds to the rotational diffusion regime that occurs at long decay times and is characteristic of anisotropic particles.

A comparison between $D_{eff}$ and $D_0$ indicates if the particles are indeed being accelerated by irradiation with the 632.8 nm laser. The calculated $D_0$ is 6.58 µm²/s and $D_{eff}$ is 8.13 µm²/s, which corresponds to an average 24% increase of the diffusion coefficient. Thus, jSNP5_Au1 are accelerating, even though they are not being excited at their SPR wavelength. The Zetasizer Nano ZS is equipped with a laser of 632.8 nm, while the SPR is around 534 nm. Lastly, the jSNP5_Au1 were moving with an average directional speed of 3.95 µm/s.

The average speed for the directional motion is dependent on the rotation relaxation time ($\tau_R$) and on the difference between the apparent translation diffusion coefficient under irradiation ($D_{eff}$) and the translation diffusion coefficient correspondent to Brownian motion ($D_0$). The jSNP5_Au1 developed directional motion upon light irradiation.

The 24% increase of the diffusion coefficient might be due to the gold nanoshell dispersity. Therefore, the creation of a more uniform gold nanoshell would be expected to lead to a greater increase of the diffusion coefficient.

From these experiments, it is possible to conclude that the presence of a uniform and complete half gold nanoshell is not a requirement to make the particles accelerate. As long as AuNPs are seeded to the SNPs surface with a reduced interparticle distance, they are capable of converting the absorbed laser energy into heat. The resulting temperature gradient was enough to induce directional motion of the particles. If a higher seed deposition density had been obtained for jSNP5_Au1, an intensified temperature gradient would be expected, inducing a higher thermophoretic force to propel the particle, which would result in particles moving with higher speeds.

## 4 Conclusions

The goal of this work was to prepare Janus nanoparticles, composed by a SNP core and a gold nanostructure in half of their surface. Irradiation of the gold nanoshell generates a thermophoretic force, propelling the Janus nanoparticle.

Janus nanoparticles were prepared by a Pickering emulsion route, and the exposed surface of the SNPs was modified with APTES to further seed AuNPs. Once AuNPs were seeded to the SNP surface, the growth of a gold nanoshell was tested by reducing chloroauric acid with different reducing agents.

The surface coverage of APTES per $nm^2$ determines the seed deposition density. Higher surface coverages translate into a high seed deposition density. A surface coverage of 15 APTES molecules/$nm^2$ was reached and TEM images revealed the deposition of AuNPs in half of the SNP surface. A uniform gold nanoshell was accomplished by reduction of chloroauric acid with formaldehyde at 55°C. These particles were analyzed by UV/Vis spectroscopy, and exhibited a strong plasmon optical resonance which was red shifted to a longer wavelength (665 nm) than the corresponding wavelength (507 nm) of AuNPs.

Motion studies were performed by DLS. The Janus nanoparticles exhibited a translational diffusion regime at short decay times and a rotational diffusion regime at long decay times. Upon irradiation with a 632.8 nm laser, a 24% increase of the translational diffusion coefficient was verified, indicating that Janus nanoparticles showed propulsion by light irradiation, with an average directional velocity of 3.95 µm/s.

In conclusion, the goal of this work was successfully achieved. The novelty comes from the preparation of a nanosystem with self-propulsion capabilities powered by light. Our system is very promising since it provides a novel nanoscale fuel-free propulsion method, that can be employed for drug delivery applications.

## 5 Future Work

It should be of great interest to tune and improve our nanomotors by trying to achieve a controllable and uniform growth of a half gold nanoshell by reduction of chloroauric acid with a non-toxic reducing agent, such as ascorbic acid or $NaBH_4$. Studies on how to control the nanoshell thickness would be important, since it would allow the tune of the plasmon resonance of the half gold nanoshell over a wide range of the electromagnetic spectrum.

In further studies, it would be interesting to test these systems in cells. To work as nanocarriers for drug delivery systems, it would be necessary to add a component that would hold and release the drug in a controllable way. This could be achieved by adding polymers to the free half surface of the silica nanoparticle or by creating a Janus nanoparticle which core was composed by a mesoporous silica nanoparticle, where the drug could be entrapped in the pores. Also, targeting capabilities could be added by the introduction of folic acid in the silica surface. Once the system is adsorbed to the cellular membrane, the propulsion provided by the thermophoretic effect would force the particles into the cell with high efficiency.

## References


(1) Walther, A.; Müller, A. H. E. Janus Particles: Synthesis, Self-Assembly, Physical Properties, and Applications. *Chem Rev* **2013**, *113* (7), 5194–5261. https://doi.org/10.1021/cr300089t.

(2) Su, H.; Hurd Price, C. A.; Jing, L.; Tian, Q.; Liu, J.; Qian, K. Janus Particles: Design, Preparation, and Biomedical Applications. *Mater Today Bio* **2019**, *4*. https://doi.org/10.1016/j.mtbio.2019.100033.

(3) Zhang, X.; Fu, Q.; Duan, H.; Song, J.; Yang, H. Janus Nanoparticles: From Fabrication to (Bio)Applications. *ACS Nano* **2021**, *15* (4), 6147–6191. https://doi.org/10.1021/acsnano.1c01146.

(4) Tadros, T. F. Emulsion Formation, Stability, and Rheology. In *Emulsion Formation and Stability*; 2013; pp 1–76.

(5) Gao, J.; Bu, X.; Zhou, S.; Wang, X.; Bilal, M.; Hassan, F. U.; Hassanzadeh, A.; Xie, G.; Chelgani, S. C. Pickering Emulsion Prepared by Nano-Silica Particles - A Comparative Study for Exploring the Effect of Various Mechanical Methods. *Ultrason Sonochem* **2022**, *83*. https://doi.org/10.1016/j.ultsonch.2022.105928.

(6) Gonzalez Ortiz, D.; Pochat-Bohatier, C.; Cambedouzou, J.; Bechelany, M.; Miele, P. Current Trends in Pickering Emulsions: Particle Morphology and Applications. *Engineering*. Elsevier Ltd April 1, 2020, pp 468–482. https://doi.org/10.1016/j.eng.2019.08.017.

(7) Zhan, Z.; Wei, F.; Zheng, J.; Yang, W.; Luo, J.; Yao, L. Recent Advances of Light-Driven Micro/Nanomotors: Toward Powerful Thrust and Precise Control. *Nanotechnol Rev* **2018**, *7* (6), 555–581. https://doi.org/10.1515/ntrev-2018-0106.

(8) Yuan, K.; Pacheco, M.; Jurado-Sánchez, B.; Escarpa, A. Design and Control of the Micromotor Swarm Toward Smart Applications. *Advanced Intelligent Systems* **2021**, *3* (6), 2100002. https://doi.org/10.1002/aisy.202100002.

(9) Pasciak, A.; Marin, R.; Abiven, L.; Pilch-Wróbel, A.; Misiak, M.; Xu, W.; Prorok, K.; Bezkrovnyi, O.; Marciniak, L.; Chanéac, C.; Gazeau, F.; Bazzi, R.; Roux, S.; Viana, B.; Lehto, V. P.; Jaque, D.; Bednarkiewicz, A. Quantitative Comparison of the Light-to-Heat Conversion Efficiency in Nanomaterials Suitable for Photothermal Therapy. *ACS Appl Mater Interfaces* **2022**. https://doi.org/10.1021/acsami.2c08013.

(10) Wang, Y. C.; Rhéaume, É.; Lesage, F.; Kakkar, A. Synthetic Methodologies to Gold Nanoshells: An Overview. *Molecules* **2018**, *23* (11). https://doi.org/10.3390/molecules23112851.

(11) Hassan, P. A.; Rana, S.; Verma, G. Making Sense of Brownian Motion: Colloid Characterization by Dynamic Light Scattering. *Langmuir* **2015**, *31* (1), 3–12. https://doi.org/10.1021/la501789z.

(12) Lee, S. W.; Nguyen, T. T. T.; van The, V.; Park, S. E. Optical Properties and Surface Morphologies of Silica-Gold Nanoshells Depending on Buffer Solutions and Reducing Agents. *Electronic Materials Letters* **2021**, *17* (5), 444–450. https://doi.org/10.1007/s13391-021-00292-x.

(13) McGlasson, A.; Bradley, L. C. Investigating Time-Dependent Active Motion of Janus Micromotors Using Dynamic Light Scattering. *Small* **2021**, *17* (52). https://doi.org/10.1002/smll.202104926.

(14) Crucho, C. I. C.; Baleizão, C.; Farinha, J. P. S. Functional Group Coverage and Conversion Quantification in Nanostructured Silica by 1H NMR. *Anal Chem* **2017**, *89* (1), 681–687. https://doi.org/10.1021/acs.analchem.6b03117.

(15) Cortie, M.; Ford, M. A Plasmon-Induced Current Loop in Gold Semi-Shells. *Nanotechnology* **2007**, *18* (23). https://doi.org/10.1088/0957-4484/18/23/235704.

(16) Jian Ye; Liesbet Lagae; Guido Maes; Gustaaf Borghs; Pol Van Dorpe. Symmetry Breaking Induced Optical Properties of Gold Open Shell Nanostructures. *Nano Lett* **2009**, *9* (12), 4049–4052. https://doi.org/10.1021/nl9022176.